# On Facilitating the use of HARDI in population studies by creating Rotation-Invariant Markers

Emmanuel Caruyer[a], Ragini Verma[a]

[a]*Section of Biomedical Image Analysis Department of Radiology University of Pennsylvania 3600 Market street, Suite 380 Philadelphia, PA 19104*

**Abstract**

We design and evaluate a novel method to compute rotationally invariant features using High Angular Resolution Diffusion Imaging (HARDI) data. These measures quantify the complexity of the angular diffusion profile modeled using a higher order model, thereby giving more information than classical diffusion tensor-derived parameters. The method is based on the spherical harmonic (SH) representation of the angular diffusion information, and is generalizable to a range of HARDI reconstruction models. These scalars are obtained as homogeneous polynomials of the SH representation of a HARDI reconstruction model. We show that finding such polynomials is equivalent to solving a large linear system of equations, and present a numerical method based on sparse matrices to efficiently solve this system. Among the solutions, we only keep a subset of algebraically independent polynomials, using an algorithm based on a numerical implementation of the Jacobian criterion. We compute a set of 12 or 25 rotationally invariant measures representative of the underlying white matter for the rank-4 or rank-6 spherical harmonics (SH) representation of the apparent diffusion coefficient (ADC)

*Email address:* Emmanuel.Caruyer@uphs.upenn.edu (Emmanuel Caruyer)
*URL:* http://www.emmanuelcaruyer.com (Emmanuel Caruyer)

profile, respectively. Synthetic data was used to investigate and quantify the difference in contrast. Real data acquired with multiple repetitions showed that within subject variation in the invariants was less than the difference across subjects - facilitating their use to study population differences. These results demonstrate that our measures are able to characterize white matter, especially complex white matter found in regions of fiber crossings and hence can be used to derive new biomarkers for HARDI and can be used for HARDI-based population analysis.
*Keywords:* Diffusion MRI, High Angular Resolution Diffusion Imaging, Biomarkers, Quantitative MR Analysis

## 1. Introduction

High angular resolution diffusion imaging (HARDI) (Frank, 2001; Özarslan and Mareci, 2003; Tuch, 2004; Descoteaux et al., 2007) has emerged as a modality to overcome the limitations of diffusion tensor imaging (DTI). The angular structure of water diffusion reveals valuable information about the underlying tissue structure, notably in the brain white matter, especially in the complex areas of fiber crossing, where HARDI shows better characterization. This richer information comes at the price of a higher complexity, both for data processing and for human interpretation. This has underlined the need for a smaller set of relevant measures that quantify and summarize this high dimensional information.

The data in HARDI are typically represented by a function on the sphere, whether it is the raw diffusion signal, the orientation distribution function (ODF), the apparent diffusion coefficient (ADC) profile, or any other function derived from the diffusion signal. Natural mathematical representations for the HARDI signal include the spherical harmonics (SH) ba-

sis (Frank, 2002; Descoteaux et al., 2006) and high-order Cartesian tensors (Özarslan and Mareci, 2003), possibly with positivity constraints (Barmpoutis et al., 2012), which correspond to homogeneous polynomials on the sphere. An alternative representation (Florack and Balmashnova, 2008) using heterogeneous polynomials was also proposed, and shown to be amenable to regularization. In this work, we are interested in measures that quantify the angular complexity of the diffusion profile. For which it is important to be rotationally invariant: from such measures, we can analyze the angular complexity of white matter configurations, irrespective of the orientation of the patient in the scanner, or the local direction of white matter pathways. The derivation of rotational invariant measures is a first step towards the creation of novel biomarkers of neurological pathologies using HARDI, by a proper statistical analysis of patient versus control populations.

Several scalar indices have been proposed in this respect. For diffusion-tensor MRI, invariants are calculated from the eigenvalues, such as the fractional anisotropy (FA) and relative anisotropy (RA) (Basser and Pierpaoli, 1996), the linear, planar and spherical measures characterizing the shape of the tensor (Westin et al., 2002). In HARDI, popular measures are the generalized fractional anisotropy (GFA) (Tuch, 2004), which can easily been computed from the spherical harmonics (SH) representation of the ODF, and the generalized anisotropy (Özarslan et al., 2005). Other groups have proposed original contributions. In Zhan et al. (2006), the authors first reorient the ODF to the orthogonal space defined by the local diffusion tensor eigenvectors, and use the SH coefficients in this space as rotational invariant measures. This method however suffers from the well-known instability of diffusion tensor decomposition, especially for oblate tensors, typical in fiber crossing configurations. From a different perspective, starting

from an SH representation of the ODF, the power spectrum is a rotation-invariant measure (Kazhdan et al., 2003). This has been used successfully for the registration of ODFs (Bloy and Verma, 2010) for instance. However, the power spectrum dramatically reduces the information, and it is shown in (Kazhdan et al., 2003) that very different shapes can have the same power spectrum. More recently, a method based on tensor contraction (Gur and Johnson, 2014), which can be seen as a generalization of the power spectrum, was presented to derive rotation invariant features computed from a SH representation of the diffusion angular information. The authors show that their invariants have a greater discriminative power, while being robust to noise. However, there is no evidence that the invariants created with this method are independent from each other, nor that they are exhaustive. Another recent approach uses the representation of a spherical function as a 4th-order tensor (Ghosh et al., 2012a). Using the analogy between 4th-order tensors in $\mathcal{R}^3$ and 2nd-order tensors in $\mathcal{R}^6$, they derive a set of 6 rotation-invariant scalars, called the basic invariants. Lately, a novel approach has been proposed (Schwab et al., 2013), that uses the mapping between a truncated SH series of a function, and the matrix representing the convolution operator by this function. They show that the spectral decomposition of this matrix provides rotational invariant measures related to this spherical function. Finally, in Nagy et al. (2013), the authors propose a family of continuous operators on spherical functions, to derive novel rotation-invariant measures, that they applied to HARDI data in the cerebral cortex.

While all these methods propose *some* rotational invariant measures, none of them give a systematic characterization of *all* rotational invariant features of a truncated SH representation of an ODF or an ADC. Yet, this is an important problem to study, since by arbitrarily retaining a partial

subset of the rotational invariant properties, we may loose important information carried by the diffusion function. This loss of information is potentially critical for the creation of new biomarkers, where pathology may be characterized by subtle changes in white matter configuration.

Acknowledging that some known rotational invariants (Ghosh et al., 2012a; Kazhdan et al., 2003) are based on homogeneous polynomials, a recent study (Ghosh et al., 2012b) proposed to compute all rotation-invariant homogeneous polynomials of the 4th-order tensor coefficients, representing a spherical function. In this work, we independently followed a similar objective, but instead we investigate rotational invariant scalar functions in the spherical harmonics (SH) coefficients. One of the advantages of using the SH representation is that they form an orthonormal basis and naturally, increasing SH rank captures increasing angular resolution features. Additionally, we present results for up to rank-6 SH, whereas the work in Ghosh et al. (2012b) is restricted to the 4th-order tensor. Our method can be applied to the apparent diffusion coefficient (ADC) profile, the orientation distribution function (ODF), or any spherical function, for any truncation order; in this article, it is illustrated on rank-4 and rank-6 SH. Hence, it is therefore generalizable to any HARDI model. The differences with prior work is presented in more detail in the discussion section.

We show that the problem of finding rotational invariant homogeneous polynomials of the spherical harmonic can be recast into solving a set of large linear systems of equations. After solving these systems and after eliminating redundant solutions, we get 12 rotational-invariant scalars representative of the underlying white matter for the rank-4 SH basis, and 25 rotation-invariant for the rank-6 SH basis. We demonstrate the applicability of these scalars on synthetic and real data, and their sensitivity to changes

in white matter. In particular, we show that the scalars we compute provide new contrasts from diffusion-weighted images, especially in the regions of complex white matter. These scalar measures can then be used in various combinations to produce biomarkers of pathology or for group-based statistical analysis.

## 2. Theory

In this section we present the theoretical approach for a comprehensive search for all rotation-invariant homogeneous polynomials. The section is organized as follows: we first introduce the notations and the definitions for the space of homogeneous polynomials, then we recall the concept of Wigner rotation matrix, which is the cornerstone of the present method. Finally, we show that the problem of finding all such invariants can be recast as a large linear system. This theoretical section is general and can be applied to any band-limited spherical function.

### *2.1. Spherical Fourier transform and Homogeneous polynomials*

In the following, we consider a function, $f$, which has a finite representation in the spherical harmonics (SH) basis:

$$\mathbf{u} \in \mathcal{S}^2, \qquad f(\mathbf{u}) = \sum_{l=0}^{L} \sum_{m=-l}^{l} \hat{f}_{l,m} Y_{l,m}(\mathbf{u}), \tag{1}$$

where $L$ is the SH rank, and $\hat{f}_{l,m}$ are its SH coefficients. In diffusion MRI, the spherical functions of interest (ADC, ODF, FOD) are real and antipodally symmetric, and we can restrict ourselves to the real, symmetric SH basis $Y_{l,m}$ as introduced in Descoteaux et al. (2006). For a given rank $L$, this basis has dimension

$$R = \frac{(L+1)(L+2)}{2}, \tag{2}$$

and the coefficients $\hat{f}_{l,m}$ can equivalently be indexed by a single index, $i$, and represented by the vector $[\hat{f}_1 \dots \hat{f}_R]^T$.

A homogeneous polynomial of degree $t$ in dimension $R$ is a function of the form

$$P(\mathbf{x}) = \sum_{i_1=1}^{R} \sum_{i_2=i_1}^{R} \dots \sum_{i_t=i_{t-1}}^{R} a_{i_1 i_2 \dots i_t}\ x_{i_1} x_{i_2} \dots x_{i_t} \tag{3}$$

The polynomial $P$ is uniquely determined by the $t$-th order, fully symmetric tensor, $\mathbb{A}$, in $\mathcal{R}^R$. The tensor $\mathbb{A}$ has full symmetry, which means that $a_{i_1 i_2 \dots i_t} = a_{i_{\sigma(1)} i_{\sigma(2)} \dots i_{\sigma(t)}}$ for any permutation $\sigma$ of $\{1, 2, \dots, t\}$. The space of $t$-th order fully symmetric tensors in $\mathcal{R}^R$ has dimension

$$D(R,t) = \binom{t+R-1}{R-1}. \tag{4}$$

For convenience, the indices $i_1, i_2, \dots, i_t$ can be contracted, and the polynomial $P[\mathbf{a}]$ is represented by its vector of coefficients, $\mathbf{a} = [a_1 \dots a_D]^T$.

The problem of finding a homogeneous polynomial, $P[\mathbf{a}]$, that is invariant to rotation of the coordinate axis of the function $f$, can be rewritten as

$$\forall \mathbf{R} \in \mathcal{SO}(3), \qquad P[\mathbf{a}](\hat{\mathbf{f}}) = P[\mathbf{a}](\widehat{\mathbf{R} \cdot \mathbf{f}}), \tag{5}$$

where the rotated function, $\mathbf{R} \cdot f$, is defined by

$$\forall \mathbf{u} \in \mathcal{S}^2, \qquad \mathbf{R} \cdot f(\mathbf{u}) = f(\mathbf{R}^T \mathbf{u}). \tag{6}$$

In the next section, we show how Wigner matrices help in rewriting the initial problem in Eq. 5.

### *2.2. Rotation and Wigner matrices*

One of the mathematical properties of spherical harmonics is that applying a rotation, $\mathbf{R}$, to the coordinate system, is equivalent to applying a

linear transform to the coefficients. This linear transform is known as the Wigner matrix, $\mathbf{W}(\mathbf{R})$, which is a block matrix (Blanco et al., 1997):

$$\widehat{\mathbf{R} \cdot f} = \mathbf{W}(\mathbf{R})\hat{f}. \tag{7}$$

Therefore, the initial problem in Eq. 5 is equivalent to finding a homogeneous polynomial, $P[\mathbf{a}]$, verifying

$$\forall \hat{\mathbf{f}} \in \mathcal{R}^R,\ \forall \mathbf{R} \in \mathcal{SO}(3), \qquad P[\mathbf{a}](\hat{\mathbf{f}}) = P[\mathbf{a}](\mathbf{W}(\mathbf{R})\hat{\mathbf{f}}). \tag{8}$$

In what follows, we show that the function on the right-hand side of Eq. 8 is also a polynomial in $\hat{\mathbf{f}}$, and give the expression of the coefficients of this transformed polynomial.

*2.3. Homogeneous polynomial and Linear transform*

If we consider the polynomial $P[\mathbf{a}]$ applied to the vector $\mathbf{x}$ that underwent a linear transform $\mathbf{W}$, we have

$$P[\mathbf{a}](\mathbf{W}\mathbf{x}) = \sum_{i_1 i_2 \ldots i_t} \mathbf{a}_{i_1 i_2 \ldots i_t} (\mathbf{W}\mathbf{x})_{i_1} (\mathbf{W}\mathbf{x})_{i_2} \ldots (\mathbf{W}\mathbf{x})_{i_t} = P[\mathbf{b}](\mathbf{x}), \tag{9}$$

where

$$\mathbf{b}_{j_1 j_2 \ldots j_t} = \sum_{i_1 i_2 \ldots i_t} \mathbf{a}_{i_1 i_2 \ldots i_t} \mathbf{W}_{i_1 j_1} \mathbf{W}_{i_2 j_2} \ldots \mathbf{W}_{i_t j_t}. \tag{10}$$

In short, this means that applying a linear transform $\mathbf{W}$ to the vector $\mathbf{x}$, is equivalent to applying a linear transform to the coefficients of the polynomial. We note $\mathbf{T}(\mathbf{W})$ the transform derived in Eq. 10, such that $\mathbf{b} = \mathbf{T}(\mathbf{W})(\mathbf{a})$.

The problem of finding a polynomial $P[\mathbf{a}]$ verifying Eq. 8 is therefore equivalent to finding a vector of coefficients $\mathbf{a}$ such that

$$\forall \mathbf{R} \in \mathcal{SO}(3), \qquad \mathbf{a} = \mathbf{T}\left(\mathbf{W}(\mathbf{R})\right)\mathbf{a}. \tag{11}$$

In what follows, we introduce a theorem which permits to rewrite the conditions in Eq. 11 into a single linear system of equations in $\mathbf{a}$.

*2.4. Linear system and sufficient condition*

**Theorem 1.** *A homogeneous polynomial $P[\mathbf{a}]$ applied to the SH coefficients of a spherical function, $f$, is unchanged after applying any rotation $\mathbf{R}$ to the coordinate axis if and only if it is unchanged by both rotations of 1rad about $x$ and about $z$.*

The proof of theorem 1 is presented in Appendix A. Combined with the previous developments, and in particular with the conditions in Eq. 11, the problem is finally equivalent to the following linear system solving,

$$\text{find } \mathbf{a} \in \mathcal{R}^{D(R,t)} \text{ such that } \mathbf{M}\mathbf{a} = \mathbf{0}, \qquad \text{where} \qquad \mathbf{M} = \begin{bmatrix} \mathbf{T}\left(\mathbf{W}(\mathbf{R}_x(1))\right) - \mathbf{I} \\ \mathbf{T}\left(\mathbf{W}(\mathbf{R}_z(1))\right) - \mathbf{I} \end{bmatrix} \tag{12}$$

where $\mathbf{I}$ is the $D(R,t) \times D(R,t)$ identity matrix, and $\mathbf{R}_x(1)$ and $\mathbf{R}_z(1)$ represent the rotations of 1rad about $x$ and $z$ axes, respectively. For a given degree $t$, the set of solutions, $\mathbf{a}$, to this linear system defines the rotationally invariant polynomials.

*2.5. Independence of solutions*

Solving the linear system in Eq. 12 will provide a family of polynomial solutions that are linearly independent in $\mathcal{R}[X_1, \ldots, X_R]$. However, at this stage, it is not guaranteed that the solutions are *algebraically* independent, since for instance the product of two solutions is also a solution. In this section, we recall how algebraic independence is defined and present a practical way to test that it is satisfied.

**Definition 1.** *A set of $k$ polynomials $P_1, \ldots, P_k$ of $\mathcal{R}[X_1, \ldots, X_R]$ are called algebraically independent if*

$$\forall Q \in \mathcal{R}[Y_1, \ldots, Y_k], \qquad Q(P_1, \ldots, P_k) = 0 \;\Rightarrow\; Q = 0.$$

Although an upper bound is known for the degree of the annihilating polynomial, $Q$ (when it exists), the computation of such a polynomial is known to be an NP hard problem (Kayal, 2009). Therefore it is not computationally efficient to try to show algebraic dependence or independence by searching for an annihilating polynomial.

However, the theorem (see Ehrenborg and Rota (1993), Th. 2.3 for a proof), known as the Jacobian criterion, states that $P_1, \ldots, P_k$ are algebraically independent if and only if the Jacobian matrix $(\partial P_i/\partial X_j)_{1\leq i\leq k, 1\leq j\leq R}$ has full rank. In order to compute this, we can use the Schwartz-Zippel polynomial identity testing lemma (Schwartz, 1980; Zippel, 1979; DeMillo and Lipton, 1978), which states that for some random $\mathbf{x} \in \mathcal{R}^R$, the Jacobian matrix has the same rank as $(\partial P_i/\partial X_j)|_{X_j=x_j}$ with high probability.

## 3. Material and methods

In what follows, we describe the method to solve the linear system of equations in Eq. 12, and subsequently extract a family of independent invariant polynomials. Finally, we relate some well-known measures to the invariants obtained with this method.

### *3.1. Solving the linear system*

As reported in Table 1, the dimension of the linear system of Eq. 12 rapidly increases with the maximum rank of the spherical harmonics, $L$, and the polynomial degree, $t$. Therefore, the complexity of general-purpose linear solvers does not scale to the size of the problem. However, it is worth observing that the structure of the problem is inherently sparse.

Indeed, due to the definition of spherical harmonics, the Wigner matrices corresponding to pure rotation about one of the Cartesian axes are sparse.

| $L$ | $R(L)$ | $D(R,t)$ | | | |
|---|---|---|---|---|---|
| | | $t=1$ | $t=2$ | $t=3$ | $t=4$ |
| 0 | 1 | **1** | **1** | **1** | **1** |
| 2 | 6 | **6** | **21** | **56** | **126** |
| 4 | 15 | **15** | **120** | **680** | **3060** |
| 6 | 28 | **28** | **406** | **4060** | **31465** |

Table 1: Dimension of the linear system of Eq. 12. The dimension increases rapidly with the truncation rank, $L$, and the polynomial degree, $t$.

As a consequence, the corresponding transform matrices $\mathbf{T}\left(\mathbf{W}(\mathbf{R}_x(1))\right)$ and $\mathbf{T}\left(\mathbf{W}(\mathbf{R}_z(1))\right)$ are sparse too, as reported in Fig. 1. This facilitates the use of adapted algorithms for solving sparse linear systems. We implemented the construction of these sparse matrices in C/Cython (Behnel et al., 2011), and we solved the linear system with ARPACK (Lehoucq et al., 1997), for which SciPy (Jones et al., 2001–) conveniently offers a Python wrapping.

### *3.2. Solutions pruning*

We propose a method, described in Algorithm 1, to keep only algebraically independent polynomials. The procedure AlgebraicIndependent tests whether a set of polynomials are algebraically independent or not, using the Jacobian criterion (see Sec. 2.5).

This pruning step greatly simplifies the set of solutions. We report in Table 2 the number of solutions before and after the pruning step. As a result, we found for rank-4 SH a total of 12 independent parameters, while the linear space of functions has dimension $R = 15$. Similarly, for rank-6 SH, we found a total of 25 independent invariants, whereas the dimension

a. Wigner matrices corresponding to rotations of 1 rad about x and z, respectively.

$W(R_x(1.0))$

$W(R_z(1.0))$

b. Matrix representing the linear system of Eq. 13 (degree t = 2).

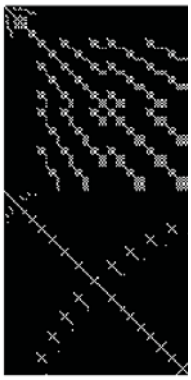

Figure 1: The Wigner matrices and the corresponding linear system of Eq. 12 are sparse. Hence they can be efficiently represented in memory, and most importantly, the system of Eq. 12 can be efficiently solved.

**Algorithm 1** SolutionsPruning(solutions)

**Require:** solutions[$L$, $t$] contains the solutions of Eq. 12.

```
indep_polys ← []
for L ∈ {0, 2, ..., L_max} do
  for t = 1 to t_max do
    for all P ∈ solutions[L, t] do
      if AlgebraicIndependent(indep_polys ∪ P) then
        indep_polys[L, t] ← indep_polys[L, t] ∪ P
      end if
    end for
  end for
end for
return indep_polys
```

| $L$ | Number of invariants | | | | |
|---|---|---|---|---|---|
| | $t=1$ | $t=2$ | $t=3$ | $t=4$ | $t=5$ |
| 0 | 1 (**1**) | 1 (**0**) | 1 (**0**) | 1 (**0**) | 1 (**0**) |
| 2 | 1 (**0**) | 2 (**1**) | 3 (**1**) | 4 (**0**) | 5 (**0**) |
| 4 | 1 (**0**) | 3 (**1**) | 7 (**3**) | 15 (**5**) | 31 (**0**) |
| 6 | 1 (**0**) | 4 (**1**) | 13 (**5**) | 46 (**7**) | N/A |

Table 2: The number of invariants before and after solution pruning (the latter appears boldface and in brackets). As a result of this simplification, the total number of invariants found for rank-4 SH went from 77 to 12, and from 141 to 25 for rank-6 SH.

of the space is 28. We recall that a rotation in $\mathcal{R}^3$ has 3 degrees of freedom, therefore this result strongly suggests that the 12 (respectively 25) invariants we found fully characterize the shape of a spherical function up to rank-4 (respectively rank-6), irrespective of its orientation. For the sake of clarity, the different steps needed to construct the set of solutions are summarized in Appendix B. Some of the solutions are reported in Appendix C.

### *3.3. Relation to known invariants*

In this section, we provide evidence that the proposed invariants encompass widely used scalar measures, namely fractional anisotropy (FA) and mean diffusivity (MD) in DTI, and generalized fractional anisotropy (GFA) in HARDI. We recall that the MD and FA of a diffusion tensor $\mathbf{D}$ can be computed as

$$\text{MD} = \frac{1}{3}\text{Tr}(\mathbf{D}), \qquad \text{and} \qquad \text{FA} = \left(\frac{3\text{Tr}(\mathbf{D}^2) - \text{Tr}(\mathbf{D})^2}{2\text{Tr}(\mathbf{D}^2)}\right)^{1/2}. \tag{13}$$

The expressions in Eq. 13 only involve $\text{Tr}(\mathbf{D})$ and $\text{Tr}(\mathbf{D}^2)$, that are homogeneous polynomials in the coefficients of the tensor. There is an isomor-

phism between the set of symmetric Cartesian tensors, and the SH basis (Özarslan and Mareci, 2003). So in essence, representing the ADC profile with its SH series coefficients, $\mathbf{c}$, with a truncation rank $L = 2$ is equivalent to using a second-order diffusion tensor model. Using this isomorphism and Eq. 13, we can write

$$\mathrm{MD} = \frac{P_{0,1}}{2\sqrt{\pi}}, \qquad \text{and} \qquad \mathrm{FA} = \left( \frac{15P_{2,2} - 12{P_{0,1}}^2}{2\left(2{P_{0,1}}^2 + 5P_{2,2}\right)} \right)^{1/2}. \tag{14}$$

This means that FA is obtained from the SH coefficients of the ADC as a simple function of two second-order polynomials.

As for the GFA of the ADC, we recall that the definition is

$$\mathrm{GFA} = \left( \frac{\int_{\mathcal{S}^2} \left( \mathrm{ADC} - \int_{\mathcal{S}^2} \mathrm{ADC} \right)^2}{\int_{\mathcal{S}^2} \mathrm{ADC}^2} \right)^{1/2} \tag{15}$$

$$= \left( \frac{P_{2,2} + P_{4,2}}{{P_{0,1}}^2 + P_{2,2} + P_{4,2}} \right)^{1/2} \tag{16}$$

where the expression in Eq. 16 can be written as a simple combination of second-order polynomials in the SH coefficients.

## 4. Experiments and Results

In this section, we present the 12 rotation invariant measures computed from the ADC profile expressed in the SH basis, truncated to rank $L = 4$, on synthetic and in vivo human brain data. The invariant measures are presented together with FA and GFA. Nest, we present a statistical analysis to investigate the reproducibility of the proposed measures on a test-retest dataset.

*4.1. Experimentation on synthetic dataset*

We computed the scalars for a synthetic configuration of two fiber populations crossing in a voxel. Water diffusion in this configuration is modeled by a discrete mixture of two Gaussian distributions, each of which is fully described by a tensor. In this setting, the fractional anisotropy of each compartment is set to 0.7, while the crossing angle increases from 0 to 90°. Diffusion-weighted signal was simulated, and we estimated the apparent diffusion coefficient (ADC) profile from the noise-free measurements. We report in Fig. 2 the values of the 25 invariants computed from the ADC profile. As expected, the scalars associated with higher spherical harmonic rank ($L = 4$ and $L = 6$) vanish whenever the crossing angle goes to zero, as this corresponds to a single fiber configuration. Besides, the curves reported in Fig. 2 suggest that the 25 invariants carry significantly different information.

In order to show that the measures are sensitive to the different configurations of white matter fiber bundles, and can characterize the complex crossing white matter, we computed the invariants on a synthetic phantom of diffusion. We created the digital phantom using *Phantomas*[1], with an arrangement of 5 cylindrical fiber bundles as illustrated on Fig. 3. The diffusion within each bundle is modeled by a restricted compartment with cylindrical boundary, and a hindered compartment. The signal for the hindered compartment is computed on the lines of Söderman and Jönsson (1995), while the hindered compartment is modeled by an anisotropic Gaussian diffusion as in the CHARMED model (Assaf and Basser, 2005). We further assume that the diffusion outside the bundles is slow ($D = 0.2\text{mm}^2 \cdot \text{s}^{-1}$)

[1] `http://www.emmanuelcaruyer.com/phantomas.php`

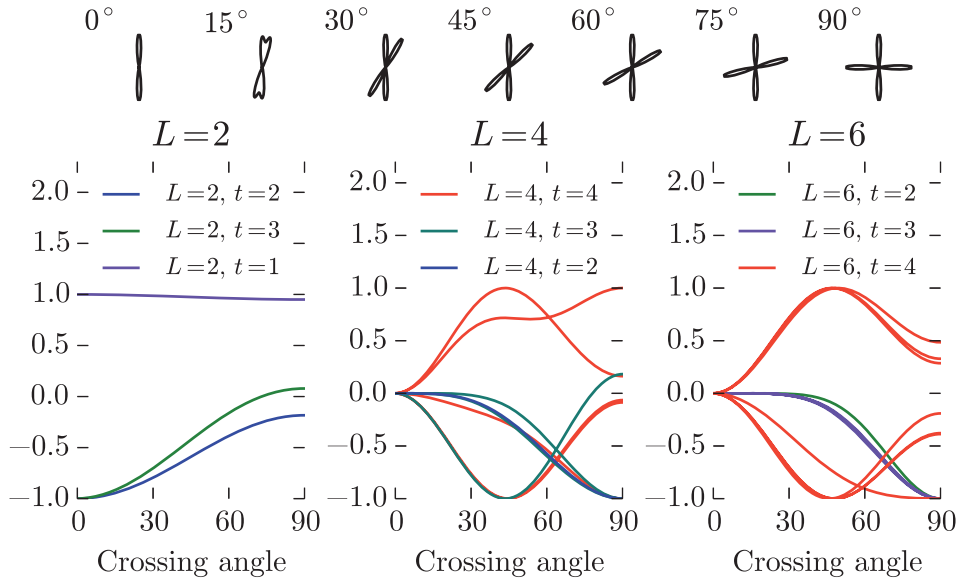


Figure 2: Top: Fiber Orientation Distribution for a synthetic configuration of crossing fibers, with increasing angle. Bottom: the corresponding ADC-based scalars, plotted against the crossing angle. The y-axis represents the value of each scalar (normalized by its maximum absolute value). The FA of each compartment is set to 0.7. We report the invariants for SH ranks $L = 2, 4, 6$ each on a separate plaot, for clarity.

and isotropic, similar to what found in brain gray matter. The partial volume and fiber orientation distributions were computed on a subdivision of $9\times9\times9$ of each voxel. We estimated the ADC profile from the noise-free signal attenuation. The 12 invariants for rank-4 SH are reported in Fig. 3. Also shown are the tensor-based fractional anisotropy (FA), as well as ADC-based generalized fractional anisoptropy (GFA), generalized anisotropy (GA) and scaled entropy (SE) (Özarslan et al., 2005) for comparison on the amount of information that is conveyed.

### *4.2. Validation on a human brain dataset*

The aim of this experiment was to show that these invariants can be consistenly computed on the same person and the variability is low compared to the variability between different people. As such they are sensitive enough for finding group differences. A group of 9 healthy subjects (6 males, 3 females, aged 31.2±4.2 years) were scanned three times with a two weeks interval between two consecutive scans. HARDI images were acquired on a Siemens 3T Verio$^{\mathrm{TM}}$ scanner using a monopolar Stejskal-Tanner diffusion weighted spin-echo, echo-planar imaging sequence (TR/TE=14.8s/111ms, 2mm isotropic voxels, $b = 3000\mathrm{s}\cdot\mathrm{mm}^{-2}$, 64 evenly distributed diffusion directions, 2 b0 images, scan time 18 minutes).

In order to correct for Rician noise, we first applied the joint linear minimum mean squared error filter (Tristán-Vega and Aja-Fernández, 2010) (using 3d Slicer (Pieper et al., 2004)) to the diffusion-weighted images. We reconstructed the ADC profile in the SH basis up to rank $L = 6$, and computed the 25 invariants, for each subject and each time step. We report on Fig. 4 the invariants for one of the subjects in the study (we only reported 3 of the 13 invariants associated with rank-6 SH, to save space on the figure).

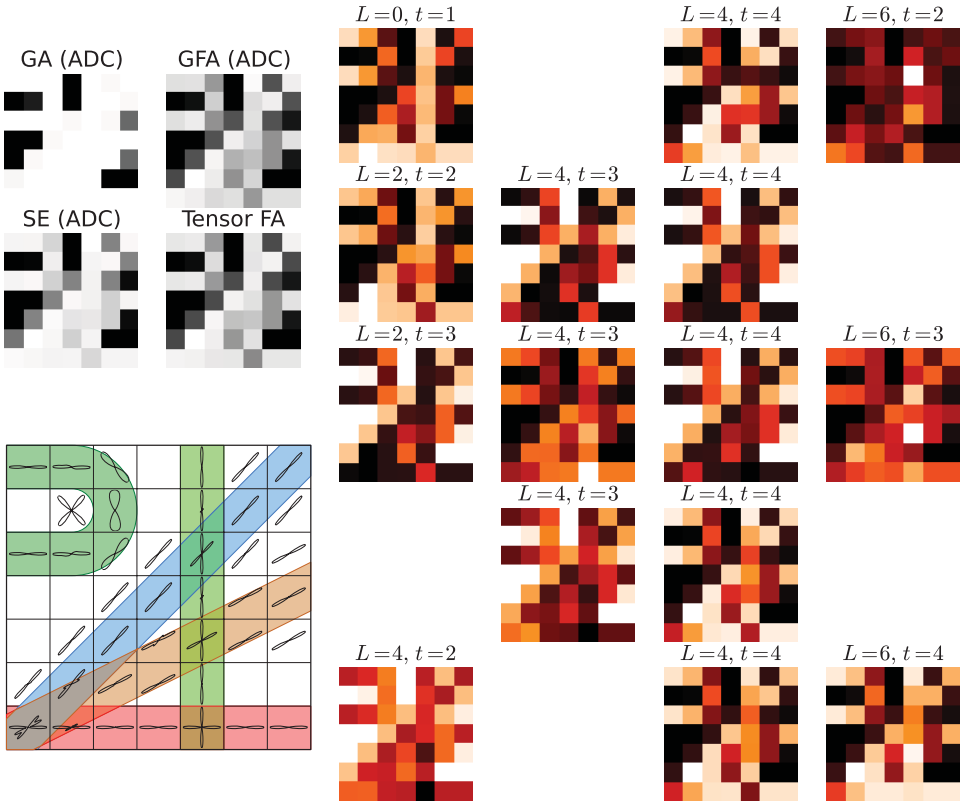


Figure 3: ADC-based invariants computed on a synthetic phantom of diffusion. Left: fiber configurations and computed fiber orientation distributions (FOD) of the tissue compartment. For visualization, the FODs have been normalized. For completeness, we also report the tensor-based fractional anisotropy (FA), the ADC-based generalized fractional anisotropy (GFA), generalized anisotropy (GA) and scaled entropy (SE). Right: the ADC-based invariants, complete up to $L = 4$; for $L = 6$, we only report 3 out of the 13 that we computed. We use gray scale for FA, GFA, GA and SE, and a color map ranging from dark red (low/negative values) to light yellow (high/positive values) for the invariant measures.

Visually, the scalar maps reported on Fig. 4 provide a set of very different images, showing contrast different from classical FA, GFA, GA and SE maps.

To analyze and compare intra-subject variability versus inter-subject variability, we performed a one-way ANalysis Of VAriance (ANOVA) test on a set of 95 regions of interest (ROI) in deep white matter from the JHU "Eve" atlas (Mori et al., 2008). To define these ROIs in subject space, we first performed a non-linear registration of the template FA to the subject FA image using DRAMMS (Ou et al., 2011). The deformation field was subsequently applied to the label map, using nearest neighbour interpolation. A visual quality check was performed on the registration results. We then computed the mean of the scalars over each ROI and performed ANOVA test on the means, where the three repetition of each subject was considered as a group. This ANOVA test is helping us to find statistical difference between subjects. The ANOVA is performed for each invariant independently, and corrected for multiple comparison over the regions using the Bonferroni method. Results of the corrected $p$-values per ROI are reported in Fig. 5.

## 5. Discussion

We presented a novel method to compute rotationally invariant measures from HARDI measurements. Although we reported ADC-based invariants throughout the Results section, the method is generalizable to compute the invariants for the ODF, or the FOD. The main reason for choosing the ADC model is that it can be seen as a higher-order extension of the second-order diffusion tensor, and therefore, the measures we compute are in a sense extensions of the FA, MD and other DTI scalars.

The method we propose here differs significantly from these previous

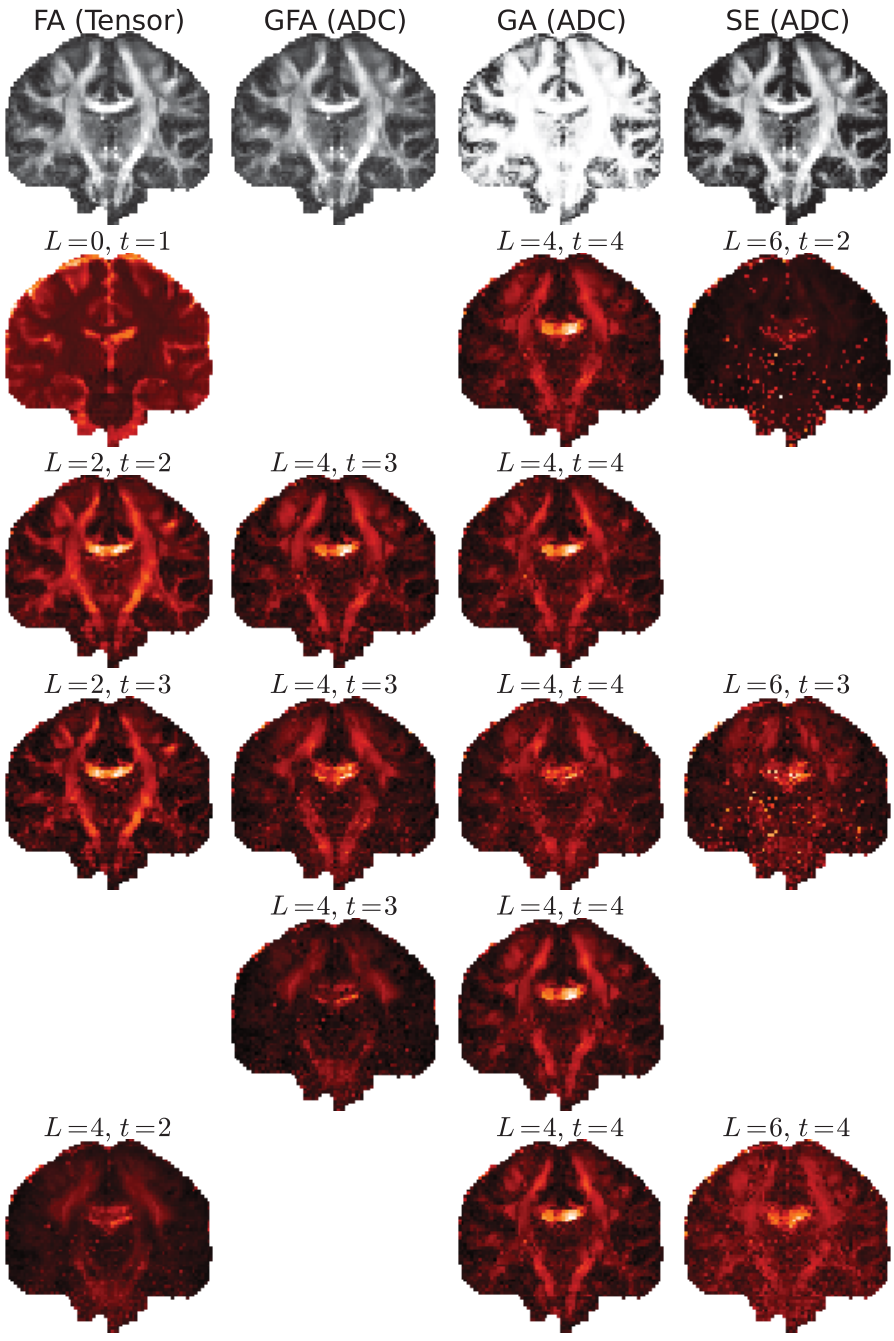


Figure 4: ADC-based invariants on a human brain. For completeness, we also report Tensor-based FA and ADC-based GFA, GA and SE. Color map range from dark red (low/negative scalar) to bright yellow (high/positive scalar). The ADC-based scalar maps show contrast different from classical FA, GFA, GA and SE maps.

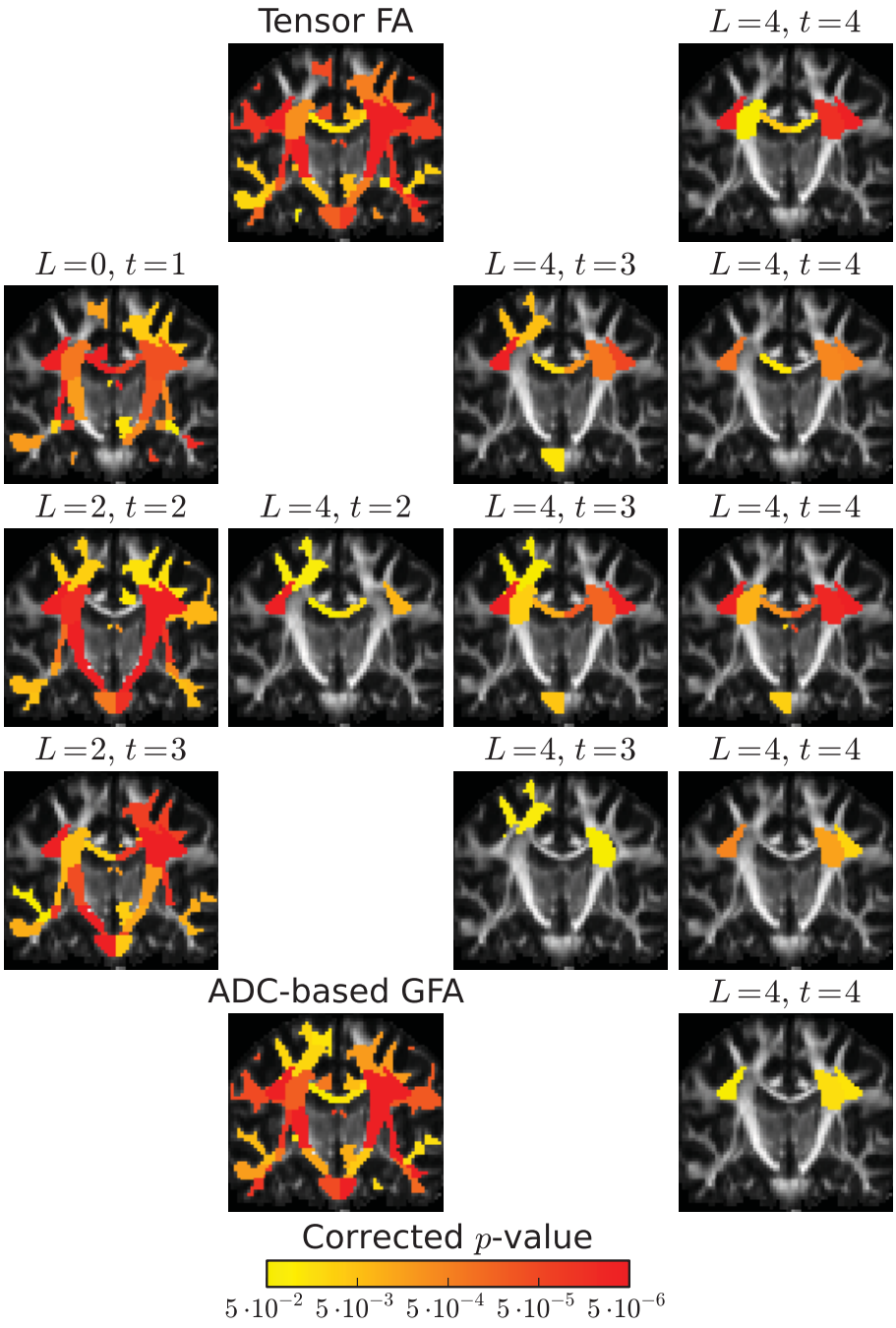


Figure 5: Results of the ANOVA test on each of the 95 ROIs in deep white matter, to compare inter-subject versus intra-subject variability on a test-retest dataset. We report the Bonferroni-corrected $p$-values for the ANOVA on each of the 12 invariants, as well as on the FA and GFA. The $p$-values represent the statistical significance of differences across subjects. The $p$-values maps are overlaid on FA for reference. The results show that the computed invariants provide measures which are significantly subject-specific in a number of regions.

studies (Ghosh et al., 2012a; Schwab et al., 2013; Gur and Johnson, 2014). These prior works share the common fact that they propose *some* rotation invariant features, whereas our method presents a systematic way to look for *all* rotation invariant features expressed as homogeneous polynomials up to a given degree. The first method (Ghosh et al., 2012a) starts from a 4th-order tensor representation of the HARDI function, and rewrites the 4th-order tensor as a 2nd-order tensor in $\mathcal{R}^6$. The authors use the fact that this transform preserves rotations, which means that a rotation applied to the original 4th-order tensor transposes into a rotation in $\mathcal{R}^6$. However, this mapping has no inverse, which means that there are rotations in $\mathcal{R}^6$ which have no transposition in the original $\mathcal{R}^3$ representation. Therefore, by imposing the solutions to be invariant to *any* rotation in $\mathcal{R}^6$, one may be over-restricting the solutions, and as a result, one is likely to find only a subset of the solutions of the problem of interest. This explains why the study in (Ghosh et al., 2012a) finds only 6 rotation invariant measures, whereas we report 12 of them for the equivalent, rank-4 SH basis, which is the expected number based on the dimension of the truncated SH space, $R = 15$, and the number degrees of freedom of a rotation, dof $= 3$. In the second method (Schwab et al., 2013), the authors use the mapping between a truncated SH series of a function, and the matrix representing the convolution operator by this function (Shirdhonkar and Jacobs, 2005). They show that a rotation in $\mathcal{R}^3$ transposes into a rotation in the space of this matrix, and subsequently find rotation-invariants measures of $f$ as rotation-invariants of this matrix, using spectral decomposition. Similarly to Ghosh et al. (2012a), the mapping they exploit between rotation matrices has no inverse, which means that the problem they solve is more constrained than the original problem, and hence they may lose some important solutions. In contrast, in

our study, we start from a rotation in $\mathcal{R}^3$, and derive its expression in the target space of invariant measures. The linear problem we solve is strictly equivalent to the original problem of finding rotationally invariant measures expressed as homogeneous polynomials in the SH coefficients. Finally, in Gur and Johnson (2014), the authors used a method of tensor contraction and Clebsch-Gordan coefficients to construct a family of rotation invariants based on the SH coefficients. They showed that this method generalizes the well-known power spectrum, but offers a greater discriminative power and higher robustness to noise. In essence, the invariants they construct are derived from tensor contraction and can be seen as polynomials, similarly to our study. However, in contrast to the present work, there is no claim that the invariants in Gur and Johnson (2014) are exhaustive, nor independent from each other.

Finally, our method is different from Ghosh et al. (2012b) in several theoretical and practical aspects. The first difference lies in the choice of the SH basis to represent the diffusion signal, where Ghosh et al. (2012b) uses a 4th-order tensor. We first outline that our method is generalizable to different SH ranks and maximum polynomial degree, and is illustrated on rank-4 as well as rank-6 SH bases. Besides, while it is true that there is an isomorphism between rank-$L$ SH and tensors of the same order, $L$, there are several mathematical properties in favor of SH basis. Most importantly, they form an orthonormal basis of functions, where the sub-domains spanned by the increasing ranks $L = \{0, 2, 4, \ldots\}$ are nested. The projection of a spherical function onto these domains provides a natural decomposition where the coefficients associated with the low-rank SH represent the smooth part of the function, and the higher rank capture the details. When they represent the apparent diffusion coefficient (ADC) profile for instance, truncated SH

to rank $L = 0$ correspond to the measurement of the isotropic ADC coefficient, truncation to rank $L = 2$ is equivalent to the diffusion tensor model, while higher ranks capture non-Gaussian diffusion. As a consequence, the scalar invariants we compute inherit from these properties and can be sorted by increasing SH rank, as well as increasing polynomial degree (see Fig. 4 for instance). Finally, the contribution in Ghosh et al. (2012b) proposes a verification of independence of the polynomial solutions *up to a given degree* (up to degree 6 in this case). In contrast, in this work we construct a set of algebraically independent polynomials, using the Jacobian criterion.

The synthetic phantom and the scalar measures reported in Fig. 3 present a range of complex white matter bundles configurations, including bending, splitting and crossing with various angles. Among the 12 invariants, some capture subtle differences that are not visible on FA and GFA maps. For instance, there is no difference between the bending configuration in A and the crossing in B in FA and GFA map, while most scalars can differentiate these configurations. This is also the case for the three crossing configurations in B, C and D. In general, the 12 invariants together are more specific than the FA and GFA.

The results reported in Fig. 5 show that the computed invariants provide measures that are significantly subject-specific in a number of ROIs. Note that we restricted this study to rank-4 SH, since the data were relatively noisy, and consequently computing rank-6 SH representation and further computing the invariants did not bring statistically significant differences in this particular dataset. Interestingly, higher-order invariants show significant differences across subjects only in the crossing bundle area of the pyramidal tract with the corpus callosum. This suggests, as expected, that the higher order invariants may capture subtle changes in these regions of

complex white matter. Although the number of samples in this population study is relatively small here (9 subjects, 3 repetitions, therefore a total of 27 samples for each ROI and each subject), these results suggest that the invariants capture individual characteristic measures in white matter. This will facilitate population analysis of HARDI data.

## 6. Conclusions

We have proposed a general method to find rotationally invariant measures of the ADC profile, based on homogeneous polynomials in the SH coefficients. As shown on synthetic and real data, these scalar measurements provide a range of new contrasts, different from FA and GFA. A study of these scalars across repeated scans shows significantly higher variability across subjects than within subject, which suggests that these scalars may be suitable for capturing group differences.

One of the possible future directions for this study is to identify which scalar, or what combination of these, can show differences between patients and controls. and therefore is suitable to build new biomarkers in HARDI. In addition, as there are a large number of features available, they can be used to train pathology specific classifiers using support vector machine, that may gain from the variation in contrast that is provided by these invariants and therefore prove suitable for building new HARDI-based pathology biomarkers. We expect that the description of a large number of scalars will pave the way for increased use of HARDI in the clinic, as it provides enhanced information over diffusion tensor imaging.

**Acknowledgments**

This research was supported by the National Institute of Health grant R01-MH-092862 to Ragini Verma.

## Appendix A. Proof of Theorem 1

In this section, we will prove Theorem 1, using two intermediate lemmas.

**Lemma 1.** *A homogeneous polynomial, $P$, applied to the SH coefficients of a spherical function, $f$, is invariant to any rotation in $\mathcal{SO}(3)$ if and only if it is invariant to any rotation about $x$, and any rotation about $z$.*

**Proof** The proof of this lemma is immediate: knowing that any rotation $\mathbf{R}$ can be written as a decomposition of three rotations:

$$\mathbf{R} = \mathbf{R}_z(\alpha)\mathbf{R}_x(\beta)\mathbf{R}_z(\gamma), \tag{A.1}$$

where $\alpha$, $\beta$ and $\gamma$ are the Euler angles.

**Lemma 2.** *A homogeneous polynomial, $P$, applied to the SH coefficients of a spherical function, $f$, is invariant to any rotation $\mathbf{R}_\mathbf{u}(\vartheta)$ about a given axis $\mathbf{u}$ if and only if it is invariant to any rotation about the rotation $\mathbf{R}_\mathbf{u}(1)$.*

**Proof** To prove this lemma, we first show that if the property is true for an angle of 1rad, then by recurrence, it is also true for any integer angle $\vartheta \in \mathcal{N}$.

Besides, as the set of integers is dense in $[0, 2\pi] \mod 2\pi$ (a property known as the Jacobi-Kronecker theorem), then for any $\vartheta \in [0, 2\pi]$, we can find two sequences of natural numbers $\vartheta_n$ and $k_n \in \mathcal{N}$ such that

$$\forall n \in \mathcal{N},\ 0 \leq \vartheta_n - 2k_n\pi \leq 2\pi, \qquad \text{and} \qquad \lim \vartheta_n - 2k_n\pi = \vartheta. \tag{A.2}$$

Finally, it is easy to see that the application $\vartheta \mapsto P(\widehat{\mathbf{R}_{\mathbf{u}}(\vartheta)} \cdot f)$ is continuous, which means that

$$P(\hat{f}) = P(\widehat{\mathbf{R}_{\mathbf{u}}(\vartheta_n)} \cdot f) \xrightarrow{n\to\infty} P(\widehat{\mathbf{R}_{\mathbf{u}}(\vartheta)} \cdot f), \tag{A.3}$$

which concludes the proof of Lemma 2.

## Appendix B. Pipeline to compute algebraicallty independent rotation-invariant polynomials

Here is a summary of the different steps to construct a family of algebraically independent rotation-invariant polynomials corresponding to rank-$L$ SH, up to a polynomial degree, $t$.

- Compute the Wigner matrices associated with rotations about $x$ and $z$ axes of 1rad. This is presented in Sec. 2.2.
- Compute the associated linear transform $\mathbf{T}$ for both matrices, as defined in Eq. 10, Sec. 2.3.
- Solve the linear system of Eq. 12 to find all linearly independent polynomial invariants of degree $t$, as presented in Sec. 2.4.
- Using Alg. 1 (Sec. 3.2), prune the solutions to keep only the polynomials which are algebraically independent with the solutions associated with lower SH rank $L' < L$, or with the same SH rank $L' = L$ but smaller polynomial degree $t' < t$.

## Appendix C. Invariant polynomial solutions

Here are some of the solutions found after the pruning step. We denote by $P^i_{L,t}$ the $i$th solution of degree $t$, corresponding to rank-$L$ SH. We omit

the superscript $i$ when there is no ambiguity (i.e. there is only one solution for this rank $L$ and this degree $t$).

$$
\begin{aligned}
P_{0,1} &= c_{0,0} \\
P_{2,2} &= \sum_{m=-2}^{2} c_{2,m}^2 \\
P_{2,3} &= c_{20}(6c_{2-2}^2 - 3c_{2-1}^2 - 2c_{20}^2 - 3c_{21}^2 + 6c_{22}^2) \\
&\quad -5.196\left(c_{2-2}(c_{2-1}^2 - c_{21}^2) + 2c_{2-1}c_{21}c_{22}\right) \\
P_{4,2} &= \sum_{m=-4}^{4} c_{4,m}^2 \\
P_{4,3}^1 &= -2.646(c_{2-2}^2 c_{4-4} + c_{22}^2 c_{4-4} + 2c_{2-2}c_{22}c_{44}) \\
&\quad -3.742(c_{2-2}c_{2-1}c_{4-3} + c_{21}c_{22}c_{4-3}) + c_{2-2}c_{21}c_{43} + c_{2-1}c_{22}c_{43}) \\
&\quad -3.464(c_{2-2}c_{20}c_{4-2} + c_{20}c_{22}c_{42}) \\
&\quad +1.414(c_{2-2}c_{2-1}c_{4-1} + c_{21}c_{22}c_{4-1} - c_{2-2}c_{21}c_{41} + c_{2-1}c_{22}c_{41}) \\
&\quad -4.899(c_{2-1}c_{20}c_{4-1} + c_{20}c_{21}c_{41}) \\
&\quad -0.447(c_{2-2}^2 c_{40} + 4c_{2-1}^2 c_{40} - 6c_{20}^2 c_{40} + 4c_{21}^2 c_{40} - c_{22}^2 c_{40}) \\
&\quad -2c_{2-1}^2 c_{4-2} + 2c_{21}^2 c_{4-2} - 4c_{2-1}c_{21}c_{42}
\end{aligned}
$$

## References


Assaf, Y., Basser, P.J., 2005. Composite hindered and restricted model of diffusion (charmed) mr imaging of the human brain. Neuroimage 27, 48–58.

Barmpoutis, A., Ho, J., Vemuri, B.C., 2012. Approximating symmetric positive semidefinite tensors of even order. SIAM journal on imaging sciences 5, 434–464.

Basser, P.J., Pierpaoli, C., 1996. Microstructural and physiological features of tissues elucidated by quantitative-diffusion-tensor MRI. Journal of Magnetic Resonance, Series B 111, 209–219. doi:http://dx.doi.org/10.1006/jmrb.1996.0086.

Behnel, S., Bradshaw, R., Citro, C., Dalcin, L., Seljebotn, D., Smith, K., 2011. Cython: The best of both worlds. Computing in Science Engineering 13, 31 –39.

Blanco, M.A., Flórez, M., Bermejo, M., 1997. Evaluation of the rotation matrices in the basis of real spherical harmonics. Journal of Molecular Structure: THEOCHEM 419, 19–27.

Bloy, L., Verma, R., 2010. Demons registration of high angular resolution diffusion images, in: ISBI, pp. 1013–1016.

DeMillo, R.A., Lipton, R.J., 1978. A probabilistic remark on algebraic program testing. Information Processing Letters 7, 193–195.

Descoteaux, M., Angelino, E., Fitzgibbons, S., Deriche, R., 2006. Apparent diffusion coefficients from high angular resolution diffusion imaging: Estimation and applications. Magnetic Resonance in Medicine 56, 395–410.

Descoteaux, M., Angelino, E., Fitzgibbons, S., Deriche, R., 2007. Regularized, fast, and robust analytical q-ball imaging. Magn. Res. Med. 58, 497–510.

Ehrenborg, R., Rota, G.C., 1993. Apolarity and canonical forms for homogeneous polynomials. European Journal of Combinatorics 14, 157–181.

Florack, L., Balmashnova, E., 2008. Two canonical representations for regularized high angular resolution diffusion imaging, in: MICCAI Workshop on Computational Diffusion MRI, New York, USA, pp. 94–105.

Frank, L.R., 2001. Anisotropy in high angular resolution diffusion-weighted mri. Magnetic Resonance in Medicine 45, 935–939.

Frank, L.R., 2002. Characterization of anisotropy in high angular resolution diffusion-weighted mri. Magnetic Resonance in Medicine 47, 1083–1099.

Ghosh, A., Papadopoulo, T., Deriche, R., 2012a. Biomarkers for hardi: 2nd & 4th order tensor invariants, in: ISBI, pp. 26–29.

Ghosh, A., Papadopoulo, T., Deriche, R., 2012b. Generalized invariants of a 4th order tensor: Building blocks for new biomarkers in dMRI, in: Proceedings of the Computation Diffusion MRI Workshop at the MICCAI Conference, Nice, France.

Gur, Y., Johnson, C.R., 2014. Generalized HARDI invariants by method of tensor contraction, in: IEEE Symposium on Biomedical Imaging, Beijing, China.

Jones, E., Oliphant, T., Peterson, P., et al., 2001–. SciPy: Open source scientific tools for Python. URL: `http://www.scipy.org/`.

Kayal, N., 2009. The complexity of the annihilating polynomial, in: Computational Complexity, 2009. CCC'09. 24th Annual IEEE Conference on, IEEE. pp. 184–193.

Kazhdan, M., Funkhouser, T., Rusinkiewicz, S., 2003. Rotation invariant SH representation of 3D shape descriptors, in: Symposium on Geometry Processing.

Lehoucq, R.B., Sorensen, D.C., Yang, C., 1997. Arpack users guide: Solution of large scale eigenvalue problems by implicitly restarted arnoldi methods.

Mori, S., Oishi, K., Jiang, H., Jiang, L., Li, X., Akhter, K., Hua, K., Faria, A.V., Mahmood, A., Woods, R., et al., 2008. Stereotaxic white matter atlas based on diffusion tensor imaging in an icbm template. Neuroimage 40, 570–582.

Nagy, Z., Alexander, D.C., Thomas, D.L., Weiskopf, N., Sereno, M.I., 2013. Using high angular resolution diffusion imaging data to discriminate cortical regions. PloS one 8, e63842.

Ou, Y., Sotiras, A., Paragios, N., Davatzikos, C., 2011. Dramms: Deformable registration via attribute matching and mutual-saliency weighting. Medical image analysis 15, 622–639.

Özarslan, E., Mareci, T.H., 2003. Generalized diffusion tensor imaging and analytical relationships between diffusion tensor imaging and high angular resolution diffusion imaging. Magnetic resonance in Medicine 50, 955–965.

Özarslan, E., Vemuri, B.C., Mareci, T.H., 2005. Generalized scalar measures for diffusion mri using trace, variance, and entropy. Magnetic Resonance in Medicine 53, 866–876.

Pieper, S., Halle, M., Kikinis, R., 2004. 3d slicer, in: Biomedical Imaging: Nano to Macro, 2004. IEEE International Symposium on, IEEE. pp. 632–635.

Schwab, E., Cetingul, H.E., Afsari, B., Yassa, M.A., Vidal, R., 2013. Rotation invariant features for hardi, in: Gee, J.C., Joshi,

S., Pohl, K.M., Wells, W.M., Zllei, L. (Eds.), Information Processing in Medical Imaging, Springer Berlin Heidelberg. pp. 705–717. doi:10.1007/978-3-642-38868-2_59.

Schwartz, J.T., 1980. Fast probabilistic algorithms for verification of polynomial identities. Journal of the ACM (JACM) 27, 701–717.

Shirdhonkar, S., Jacobs, D.W., 2005. Non-negative lighting and specular object recognition, in: Computer Vision, 2005. ICCV 2005. Tenth IEEE International Conference on, IEEE. pp. 1323–1330.

Söderman, O., Jönsson, B., 1995. Restricted diffusion in cylindrical geometry. Journal of Magnetic Resonance, Series A 117, 94–97.

Tristán-Vega, A., Aja-Fernández, S., 2010. Dwi filtering using joint information for dti and hardi. Medical Image Analysis 14, 205–218.

Tuch, D., 2004. Q-ball imaging. Magnetic Resonance in Medicine 52, 1358–1372.

Westin, C.F., Maier, S.E., Mamata, H., Nabavi, A., Jolesz, F.A., Kikinis, R., 2002. Processing and visualization for diffusion tensor mri. Medical image analysis 6, 93–108.

Zhan, W., Stein, E.A., Yang, Y., 2006. A rotation-invariant spherical harmonic decomposition method for mapping intravoxel multiple fiber structures. Neuroimage 29, 1212–1223.

Zippel, R., 1979. Probabilistic algorithms for sparse polynomials. Springer.

*Graphical Abstract

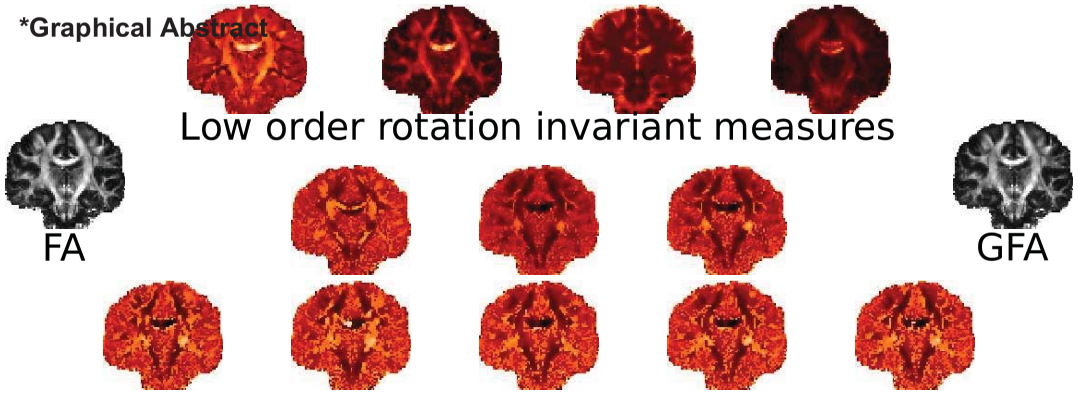

## Highlights

- A general method to extract rotation-invariant measures in HARDI
- These measures capture subtle differences not shown on FA or GFA maps
- The invariants are shown to be reproducible across scan repetitions
- The invariants are able to capture subject-specific information.